Pathology Dynamics in Healthy-Toxic Protein Interaction and the Multiscale Analysis of Neurodegenerative Diseases

Swadesh Pal[1] and Roderick Melnik[1,2(✉)]

[1] MS2Discovery Interdisciplinary Research Institute, Wilfrid Laurier University, Waterloo, Canada
rmelnik@wlu.ca
[2] BCAM-Basque Center for Applied Mathematics, Bilbao, Spain

Abstract. Neurodegenerative diseases are frequently associated with aggregation and propagation of toxic proteins. In particular, it is well known that along with amyloid-beta, the tau protein is also driving Alzheimer's disease. Multiscale reaction-diffusion models can assist in our better understanding of the evolution of the disease. Based on a coarse-graining procedure of the continuous model and taking advantage of the brain data connectome, a computationally challenging network mathematical model has been described where the edges of the network are the axonal bundles in white-matter tracts. Further, we have modified the heterodimer model in such a way that it can now capture some of the critical characteristics of this evolution such as the conversion time from healthy to toxic proteins. Finally, we have analyzed the modified model theoretically and validated the theoretical findings with numerical simulations.

Keywords: Alzheimer's disease · Coupled multiscale models · Amyloid-beta and tau proteins · Neurodegenerative disorders · Holling type-II

1 Introduction

Alzheimer's disease (AD) is an example of a neurodegenerative disease, associated with aggregation and propagation of toxic proteins [1]. Initially, the "amyloid cascade hypothesis" has dominated for the treatments [2,3]. However, due to the failures of large clinical trials, researchers started focussing on some other mechanisms. It is now well accepted that the tau-protein (τP) is a viable alternative to the "amyloid cascade hypothesis".

The τP plays a prominent role as a secondary agent in the disease development. For example, (i) frontotemporal lobar degeneration is mostly dominated by τP spreading [4], (ii) neurofibrillary tangles (NFT) are correlated in brain atrophy in AD [5,6], (iii) lower τP concentration prevents neuronal loss [7], (iv) τP also reduces neural activity [8], etc. This helps to explain the relative lack of clinical improvements. There is an open debate in the literature on the roles of $A\beta$ proteopathy and τP tauopathy in AD but it is clear by now that "the amyloid $- \beta - \tau$ nexus is central to disease-specific diagnosis, prevention and treatment" [9]. In recent years, many researchers have focussed on $A\beta$ and τP interaction. Moreover, in neurodegenerative diseases, the protein-protein interactions become a key for understanding both spreading and toxicity of the proteins [10–13]. There are some crucial observations specific to AD [10,14]: (i) the seeding of new toxic τP is enhanced by the presence of $A\beta$, (ii) the toxicity of $A\beta$ depends on the presence of τP, and (iii) $A\beta$ and τP amplify each other's toxic effects.

Mathematical models are widely used for the interpretation of biological processes, and this field is not an exception. Building on earlier advances [15–20], we analyze AD by a deterministic mathematical modelling approach and predict the dynamics of the disease based on several novel features of our model. Recall that the heterodimer model describes the interaction between the healthy and toxic proteins [21–25]. In the heterodimer model, with an increase in the healthy protein density, the toxic protein conversion increases. We have modified that linear conversion term to include nonlinear effects via Holling type-II functional response. In this case, the toxic protein's conversion rate remains constant with an increase in the healthy protein density. This modification incorporates the reaction time (conversion from healthy protein to toxic protein). AD is itself a complex and multiscale disease. The introduction of the reaction time, along with the conventional wave propagation times, reflects a multiscale character of the modified model. We have considered two modified coupled heterodimer systems for healthy-toxic interactions for both proteins, $A\beta$ and τP, along with a single balance interaction term. This study identifies two types of disease propagation modes depending on the parameters: primary tauopathy and secondary tauopathy.

Finally, we note that a network mathematical model can be constructed from the brain data by a coarse-graining procedure of the continuous model (e.g., [14]). In this case, we need to define the network nodes in the region or domain where we are interested to see the dynamics. The edges of the network are the axonal bundles in white-matter tracts. Here, the network model in the brain connectome becomes an undirected weighted graph, and the weights of the graph are used to construct the adjacency matrix and hence the Laplacian of the graph. Studying AD in the whole brain connectome is computationally very challenging. One of the efficient and logical ways to proceed is to investigate AD in the brain connectome by fixing some crucial nodes and edges, which we are currently undertaking. In the current manuscript, we provide a brief description of such a network model, but our main focus here is to establish the speed of

wave propagation of toxic fronts of the two modes of primary and secondary tauopathies for the modified reaction-diffusion model.

This manuscript is organized as follows. In Sect. 2, we briefly discuss the heterodimer model and its modification. Temporal behaviour of the modified model is analyzed in Sect. 3, focussing on possible stationary points and linear stability. In Sect. 4, we provide results on the wave propagation described by a simplified model, specific to stationary states. Section 6 is devoted to a detailed analysis of the AD propagation in terms of primary and secondary tauopathies. Concluding remarks are given in Sect. 7.

2   Mathematical Model

We first consider the usual heterodimer model for the healthy and toxic variants of the proteins $A\beta$ and τP. Let Ω be a spatial domain in $\mathbb{R}^3$. For $\mathbf{x} \in \Omega$ and time $t \in \mathbb{R}^+$, let $u = u(\mathbf{x}, t)$ and $\widetilde{u} = \widetilde{u}(\mathbf{x}, t)$ be healthy and toxic concentrations of the protein $A\beta$, respectively. Similarly, we denote $v = v(\mathbf{x}, t)$ and $\widetilde{v} = \widetilde{v}(\mathbf{x}, t)$ the healthy and toxic concentrations of τP, respectively. The concentration evolution is then given by the following system of coupled partial differential equations [14, 22]:

$$\frac{\partial u}{\partial t} = \nabla \cdot (\mathbf{D_1} \nabla u) + a_0 - a_1 u - a_2 u \widetilde{u}, \tag{1a}$$

$$\frac{\partial \widetilde{u}}{\partial t} = \nabla \cdot (\widetilde{\mathbf{D}}_1 \nabla \widetilde{u}) - \widetilde{a}_1 \widetilde{u} + a_2 u \widetilde{u}, \tag{1b}$$

$$\frac{\partial v}{\partial t} = \nabla \cdot (\mathbf{D_2} \nabla v) + b_0 - b_1 v - b_2 v \widetilde{v} - b_3 \widetilde{u} v \widetilde{v}, \tag{1c}$$

$$\frac{\partial \widetilde{v}}{\partial t} = \nabla \cdot (\widetilde{\mathbf{D}}_2 \nabla \widetilde{v}) - \widetilde{b}_1 \widetilde{v} + b_2 v \widetilde{v} + b_3 \widetilde{u} v \widetilde{v}. \tag{1d}$$

In system (1), a_0 and b_0 are the mean production rates of healthy proteins, $a_1, b_1, \widetilde{a}_1$ and $\widetilde{b}_1$ are the mean clearance rates of healthy and toxic proteins, and a_2 and b_2 represent the mean conversion rates of healthy proteins to toxic proteins. The parameter b_3 is the coupling constant between the two proteins $A\beta$ and τP. Further, $\mathbf{D}_1, \widetilde{\mathbf{D}}_1, \mathbf{D}_2$ and $\widetilde{\mathbf{D}}_2$ are the diffusion tensors which characterize the spreading of each proteins. For the isometric diffusion, the diffusion tensor is $\nabla \cdot (\mathbf{D_1} \nabla u) = D_1 \Delta u$, the usual Laplacian operator (similarly for $\widetilde{u}$, v and $\widetilde{v}$). We assume that all variables and initial conditions are non-negative and also all the parameters to be strictly positive.

Here, the healthy protein is approached by the toxic protein, and after transitions, a healthy protein is converted into a toxic state. In the current formulation, we have assumed that the probability of a given toxic protein encountering healthy protein in a fixed time interval T_t, within a fixed spatial region, depends linearly on the healthy protein density. In this case, the total density of the healthy proteins u converted by the toxic proteins $\widetilde{u}$ can be expressed as $\widetilde{u} = aT_s u$, following the Holling functional response idea [26]. The parameter T_s is the time to getting contact with each other and a is a proportionality constant.

If there is no reaction time, then $T_s = T_t$ and hence we get a linear conversion rate $\widetilde{u} = aT_t u$. Now, if each toxic protein requires a reaction time h for healthy proteins that are converted, then the time available to getting contact becomes $T_s = T_t - h\widetilde{u}$. Therefore, $\widetilde{u} = a(T_t - h\widetilde{u})u$, hence $\widetilde{u} = aT_t u/(1 + ahu)$, which is a nonlinear conversion rate. So, we modify the above model (1) as follows:

$$\frac{\partial u}{\partial t} = \nabla \cdot (\mathbf{D_1} \nabla u) + a_0 - a_1 u - \frac{a_2 u}{1 + e_1 u} \widetilde{u}, \tag{2a}$$

$$\frac{\partial \widetilde{u}}{\partial t} = \nabla \cdot (\widetilde{\mathbf{D}}_1 \nabla \widetilde{u}) - \widetilde{a}_1 \widetilde{u} + \frac{a_2 u}{1 + e_1 u} \widetilde{u}, \tag{2b}$$

$$\frac{\partial v}{\partial t} = \nabla \cdot (\mathbf{D_2} \nabla v) + b_0 - b_1 v - \frac{b_2 v}{1 + e_2 v} \widetilde{v} - b_3 \widetilde{u} v \widetilde{v}, \tag{2c}$$

$$\frac{\partial \widetilde{v}}{\partial t} = \nabla \cdot (\widetilde{\mathbf{D}}_2 \nabla \widetilde{v}) - \widetilde{b}_1 \widetilde{v} + \frac{b_2 v}{1 + e_2 v} \widetilde{v} + b_3 \widetilde{u} v \widetilde{v}, \tag{2d}$$

where e_1 ($= a_\beta h_\beta$) and e_2 ($= a_\tau h_\tau$) are dimensionless parameters. We use no-flux boundary conditions and non-negative initial conditions. Here, in model (2), the rate of conversion of the healthy protein by the toxic protein increases as the healthy protein density increases, but eventually it saturates at the level where the rate of conversion remains constant regardless of increases in healthy protein density. On the other hand, in model (1), the rate of conversion of the healthy protein by the toxic protein rises constantly with an increase in the healthy protein density.

3   Temporal Dynamics

For studying the wave propagation based on the reaction-diffusion model (2), we will first find homogeneous steady-states of the system. The homogeneous steady-states of the system (2) can be determined by finding the equilibrium points of the following system

$$\frac{du}{dt} = a_0 - a_1 u - \frac{a_2 u}{1 + e_1 u} \widetilde{u}, \tag{3a}$$

$$\frac{d\widetilde{u}}{dt} = -\widetilde{a}_1 \widetilde{u} + \frac{a_2 u}{1 + e_1 u} \widetilde{u}, \tag{3b}$$

$$\frac{dv}{dt} = b_0 - b_1 v - \frac{b_2 v}{1 + e_2 v} \widetilde{v} - b_3 \widetilde{u} v \widetilde{v}, \tag{3c}$$

$$\frac{d\widetilde{v}}{dt} = -\widetilde{b}_1 \widetilde{v} + \frac{b_2 v}{1 + e_2 v} \widetilde{v} + b_3 \widetilde{u} v \widetilde{v}, \tag{3d}$$

with non-negative initial conditions.

3.1   Stationary Points

The system (3) always has a disease-free state called a healthy stationary state. Depending on the parameter values, the system may possess more stationary points. We summarise each possible stationary state in the following:

1. Healthy $A\beta$ - healthy τP: It is the trivial stationary state and is given by

$$(u_1, \widetilde{u}_1, v_1, \widetilde{v}_1) = \left(\frac{a_0}{a_1}, 0, \frac{b_0}{b_1}, 0 \right). \tag{4}$$

This stationary state is the same for both systems, (1) and (2), due to zero toxic loads.

2. Healthy $A\beta$ - toxic τP: The stationary state of "healthy $A\beta$ - toxic τP" is given by

$$(u_2, \widetilde{u}_2, v_2, \widetilde{v}_2) = \left(\frac{a_0}{a_1}, 0, \frac{\widetilde{b}_1}{b_2 - e_2\widetilde{b}_1}, \frac{b_0(b_2 - e_2\widetilde{b}_1) - b_1\widetilde{b}_1}{\widetilde{b}_1(b_2 - e_2\widetilde{b}_1)} \right). \tag{5}$$

For the non-negativity of the stationary point (5), we must have $b_2 > e_2\widetilde{b}_1$ and $b_0/b_1 \geq \widetilde{b}_1/(b_2 - e_2\widetilde{b}_1)$.

3. Toxic $A\beta$ - healthy τP: The stationary state of "toxic $A\beta$ - healthy τP" is given by

$$(u_3, \widetilde{u}_3, v_3, \widetilde{v}_3) = \left(\frac{\widetilde{a}_1}{a_2 - e_1\widetilde{a}_1}, \frac{a_0(a_2 - e_1\widetilde{a}_1) - a_1\widetilde{a}_1}{\widetilde{a}_1(a_2 - e_1\widetilde{a}_1)}, \frac{b_0}{b_1}, 0 \right). \tag{6}$$

For the non-negativity of the stationary point (6), we must have $a_2 > e_1\widetilde{a}_1$ and $a_0/a_1 \geq \widetilde{a}_1/(a_2 - e_1\widetilde{a}_1)$.

4. Toxic $A\beta$ - toxic τP: Suppose $(u_4, \widetilde{u}_4, v_4, \widetilde{v}_4)$ is a stationary state of the "toxic $A\beta$ - toxic τP" type. In this case, we obtain $u_4 = u_3$, $\widetilde{u}_4 = \widetilde{u}_3$, $\widetilde{v}_4 = (b_0 - b_1v_4)/\widetilde{b}_1$ and v_4 satisfy the quadratic equation

$$b_3e_2\widetilde{u}_4v_4^2 + (b_3\widetilde{u}_4 - e_2\widetilde{b}_1 + b_2)v_4 - \widetilde{b}_1 = 0. \tag{7}$$

The equation (7) always has a real positive solution. For the uniqueness of v_4, we must have $b_3\widetilde{u}_4 - e_2\widetilde{b}_1 + b_2 \geq 0$. Also, for the positivity of $\widetilde{v}_4$, we need $v_4 < b_0/b_1$.

Note that under small perturbations of any one of these stationary points, the trajectories may or may not come to that stationary point. Next, we examine this situation in more detail by the linear stability analysis.

3.2   Linear Stability Analysis

For the stability analysis, we linearize the system (3) about any of the stationary points $(u_*, \widetilde{u}_*, v_*, \widetilde{v}_*)$. The coefficient matrix $\mathbf{M}$ of the resulting system is the Jacobian matrix of the system (3) and is given by

$$\begin{bmatrix} -a_1 - \frac{a_2\widetilde{u}_*}{(1+e_1u_*)^2} & -\frac{a_2u_*}{1+e_1u_*} & 0 & 0 \\ \frac{a_2\widetilde{u}_*}{(1+e_1u_*)^2} & \frac{a_2u_*}{1+e_1u_*} - \widetilde{a}_1 & 0 & 0 \\ 0 & -b_3v_*\widetilde{v}_* & -b_1 - \frac{b_2\widetilde{v}_*}{(1+e_2v_*)^2} - b_3\widetilde{u}_*\widetilde{v}_* & -\frac{b_2v_*}{1+e_2v_*} - b_3\widetilde{u}_*v_* \\ 0 & b_3v_*\widetilde{v}_* & \frac{b_2\widetilde{v}_*}{(1+e_2v_*)^2} + b_3\widetilde{u}_*\widetilde{v}_* & \frac{b_2v_*}{1+e_2v_*} + b_3\widetilde{u}_*v_* - \widetilde{b}_1 \end{bmatrix}. \tag{8}$$

Now, the eigenvalues of the Jacobian matrix $\mathbf{M}$ are given by

$$\lambda_1 = -\frac{1}{2}(B + \sqrt{B^2 - 4C}), \lambda_2 = -\frac{1}{2}(B - \sqrt{B^2 - 4C}),$$

$$\lambda_3 = -\frac{1}{2}(\widehat{B} + \sqrt{\widehat{B}^2 - 4\widehat{C}}), \lambda_4 = -\frac{1}{2}(\widehat{B} - \sqrt{\widehat{B}^2 - 4\widehat{C}}),$$

where $B = a_1 + \widetilde{a}_1 + a_2\widetilde{u}_*/(1+e_1u_*)^2 - a_2u_*/(1+e_1u_*), C = a_1\widetilde{a}_1 + \widetilde{a}_1a_2\widetilde{u}_*/(1+e_1u_*)^2 - a_1a_2u_*/(1+e_1u_*), \widehat{B} = b_1 + \widetilde{b}_1 + b_3\widetilde{u}_*(\widetilde{v}_* - v_*) + b_2\widetilde{v}_*/(1+e_2v_*)^2 - b_2v_*/(1+e_2v_*)$ and $\widehat{C} = b_1\widetilde{b}_1 + b_3\widetilde{u}_*(\widetilde{b}_1\widetilde{v}_* - b_1v_*) + \widetilde{b}_1b_2\widetilde{v}_*/(1+e_2v_*)^2 - b_1b_2v_*/(1+e_2v_*)$.

For each of the stationary points, we find the Jacobian matrix $\mathbf{M}$ and all its eigenvalues $\lambda_i, i = 1, 2, 3, 4$. Hence, the conclusion can be drawn easily, because for a given stationary point, if all the eigenvalues have negative real parts, this stationary point is stable, otherwise it is unstable.

4   Wave Propagation

We analyze travelling wave solutions of the spatio-temporal model (2) in one dimension $(\Omega = \mathbb{R})$ connecting any two stationary states $(u_i, \widetilde{u}_i, v_i, \widetilde{v}_i), i = 1, 2, 3, 4$ [21]. First, we consider the travelling wave emanating from healthy stationary state $(u_1, \widetilde{u}_1, v_1, \widetilde{v}_1)$ and connecting to $(u_2, \widetilde{u}_2, v_2, \widetilde{v}_2)$. For analysing the travelling wave fronts, we linearize the spatio-temporal model (2) around the healthy stationary state which leads to the following uncoupled system

$$\frac{\partial \widetilde{u}}{\partial t} = \widetilde{d}_1 \frac{\partial^2 \widetilde{u}}{\partial x^2} + \frac{a_2u_1}{1 + e_1u_1} - \widetilde{a}_1, \tag{9a}$$

$$\frac{\partial \widetilde{v}}{\partial t} = \widetilde{d}_2 \frac{\partial^2 \widetilde{v}}{\partial x^2} + \frac{b_2v_1}{1 + e_2v_1} - \widetilde{b}_1. \tag{9b}$$

Firstly, for the travelling wave solution, we substitute $\widetilde{u}(x, t) = \widetilde{u}(x - ct) \equiv \widetilde{u}(z), \widetilde{v}(x, t) = \widetilde{v}(x - ct) \equiv \widetilde{v}(z)$ in (9) and will look for linear solutions of the form $\widetilde{u} = C_1\exp(\lambda z), \widetilde{v} = C_2\exp(\lambda z)$. Then, the minimum wave speeds $c_{\min}$ are given by

$$c_\beta^{(12)} = 0 \text{ and } c_\tau^{(12)} = 2\sqrt{\widetilde{d}_2\left(\frac{b_2v_1}{1 + e_2v_1} - \widetilde{b}_1\right)}. \tag{10}$$

Here, $c_\beta^{(ij)}$ and $c_\tau^{(ij)}$ denote the speeds of the front from state i to the state j for the $A\beta$ fields $(u, \widetilde{u})$ and τP fields $(v, \widetilde{v})$, respectively.

Similarly, the minimum wave speeds for the travelling wave fronts emanating from healthy stationary state $(u_1, \widetilde{u}_1, v_1, \widetilde{v}_1)$ and connecting to $(u_3, \widetilde{u}_3, v_3, \widetilde{v}_3)$ are given by

$$c_\beta^{(13)} = 2\sqrt{\widetilde{d}_1\left(\frac{a_2u_1}{1 + e_1u_1} - \widetilde{a}_1\right)} \text{ and } c_\tau^{(13)} = 0. \tag{11}$$

Also, we have

$$c_\beta^{(14)} = c_\beta^{(13)} \text{ and } c_\tau^{(14)} = c_\tau^{(12)}. \tag{12}$$

Secondly, we consider the travelling wave emanating from the stationary state $(u_3, \widetilde{u}_3, v_3, \widetilde{v}_3)$ and connecting to $(u_4, \widetilde{u}_4, v_4, \widetilde{v}_4)$. We linearize the spatio-temporal model (2) around $(u_3, \widetilde{u}_3, v_3, \widetilde{v}_3)$ and repeat the same techniques to deduce that

$$c_\beta^{(34)} = 0 \text{ and } c_\tau^{(34)} = 2\sqrt{\widetilde{d}_2\left(\frac{b_2 v_3}{1 + e_2 v_3} + b_3\widetilde{u}_3 v_3 - \widetilde{b}_1\right)}. \tag{13}$$

5 Network Mathematical Model

Based on a coarse-graining procedure of the continuous model and taking advantage of the brain data, a network mathematical model can be constructed where the edges of the network are the axonal bundles in white-matter tracts (e.g., [14]). The choice of the network nodes is carried out in the region of interest and in what follows we describe the network mathematical model corresponding to the modified continuous model (2) for the brain data connectome [27]. The latter can be modelled by the coarse-grain model of the continuous system. Specifically, it is a weighted graph $\mathcal{G}$ with V nodes and E edges defined in a domain Ω. The weights of the graph $\mathcal{G}$ are represented by the adjacency matrix $\mathbf{W}$ which provides a way to construct the graph of the Laplacian. For $i, j = 1, 2, 3, \ldots, V$, the elements of $\mathbf{W}$ are

$$W_{ij} = \frac{n_{ij}}{l_{ij}^2},$$

where n_{ij} is the mean fiber number and l_{ij}^2 is the mean length squared between the nodes i and j. We define the graph of the Laplacian $\mathbf{L}$ as

$$L_{ij} = \rho(D_{ii} - W_{ij}), \quad i, j = 1, 2, 3, \ldots, V,$$

where ρ is the diffusion coefficient and $D_{ii} = \sum_{j=1}^{V} W_{ij}$ is the elements of the diagonal weighted degree matrix. Now, we are ready to build a network mathematical model in the graph $\mathcal{G}$.

At the node j, let $(u_j, \widetilde{u}_j)$ be the concentrations of healthy and toxic $A\beta$ proteins, respectively, whereas $(v_j, \widetilde{v}_j)$ be the concentrations of healthy and toxic τP proteins, respectively. Then, for all the nodes $j = 1, 2, 3, \ldots, V$, the network equations corresponding to the continuous model (2) is a system of first order differential equations and it is given by

$$\frac{du_j}{dt} = -\sum_{k=1}^{V} L_{jk} u_k + a_0 - a_1 u_j - \frac{a_2 u_j}{1 + e_1 u_j}\widetilde{u}_j, \tag{14a}$$

$$\frac{d\widetilde{u}_j}{dt} = -\sum_{k=1}^{V} L_{jk}\widetilde{u}_k - \widetilde{a}_1\widetilde{u}_j + \frac{a_2 u_j}{1 + e_1 u_j}\widetilde{u}_j, \tag{14b}$$

$$\frac{dv_j}{dt} = -\sum_{k=1}^{V} L_{jk} v_k + b_0 - b_1 v_j - \frac{b_2 v_j}{1 + e_2 v_j}\widetilde{v}_j - b_3\widetilde{u}_j v_j\widetilde{v}_j, \tag{14c}$$

$$\frac{d\widetilde{v}_j}{dt} = -\sum_{k=1}^{V} L_{jk}\widetilde{v}_k - \widetilde{b}_1\widetilde{v}_j + \frac{b_2 v_j}{1 + e_2 v_j}\widetilde{v}_j + b_3\widetilde{u}_j v_j\widetilde{v}_j, \tag{14d}$$

with non-negative initial conditions.

6   Results and Discussion

A "healthy $A\beta$ - healthy τP" stationary state satisfies $\widetilde{u} = \widetilde{v} = 0$. The non-existence of a physically relevant healthy state occurs due to a failure of healthy clearance, which is either with an $A\beta$ clearance or with a τP clearance. To start with, we consider the following balance of clearance inequalities:

$$\frac{a_0}{a_1} < \frac{\widetilde{a}_1}{a_2 - e_1\widetilde{a}_1}, \ \frac{b_0}{b_1} < \frac{\widetilde{b}_1}{b_2 - e_2\widetilde{b}_1}. \tag{15}$$

Now, if (15) holds for the stationary point $(u_1, \widetilde{u}_1, v_1, \widetilde{v}_1)$ in (4), then all the eigenvalues corresponding to the Jacobian matrix $\mathbf{M}$ have negative real parts. So, given the small amounts of the production of toxic $A\beta$ or toxic τP, or excess amounts of the production of healthy $A\beta$ or healthy τP, the system would be approaching towards the "healthy $A\beta$- healthy τP" stationary state.

Due to the failure of the clearance inequality (15), a transcritical bifurcation occurs for the homogeneous system (3). Hence, all the other stationary states $(u_i, \widetilde{u}_i, v_i, \widetilde{v}_i), i = 2, 3, 4$ are physically meaningful and a pathological development becomes possible. Motivated by [14], we fix the parameter values as $a_0 = a_1 = a_2 = b_0 = b_1 = b_2 = 1$ and $e_1 = e_2 = 0.1$. Now, we fix $\widetilde{a}_1 = 3/4, \widetilde{b}_1 = 4/3$ and we take b_3 as the bifurcation parameter. For $b_3 < 1.575$, the system has only two stationary points $(u_1, \widetilde{u}_1, v_1, \widetilde{v}_1)$ and $(u_3, \widetilde{u}_3, v_3, \widetilde{v}_3)$. The equilibrium point $(u_1, \widetilde{u}_1, v_1, \widetilde{v}_1)$ is saddle and $(u_3, \widetilde{u}_3, v_3, \widetilde{v}_3)$ is stable. A non-trivial stationary point $(u_4, \widetilde{u}_4, v_4, \widetilde{v}_4)$ is generated through a transcritical bifurcation at $b_3 = 1.575$. Then $(u_3, \widetilde{u}_3, v_3, \widetilde{v}_3)$ changes its stability to $(u_4, \widetilde{u}_4, v_4, \widetilde{v}_4)$ and becomes saddle (see Fig. 1).

These results could lead to a number of important observations. For example, due to the instability of the healthy stationary state of the system (3), a proteopathic brain patient would be progressing toward a disease state. The actual state would depend on the parameter values. If $b_0/b_1 \geq \widetilde{b}_1/(b_2 - e_2\widetilde{b}_1)$ holds, then $(u_2, \widetilde{u}_2, v_2, \widetilde{v}_2)$ exists and if $a_0/a_1 \geq \widetilde{a}_1/(a_2 - e_1\widetilde{a}_1)$ holds, then $(u_3, \widetilde{u}_3, v_3, \widetilde{v}_3)$ exists. Sometimes both the relations hold simultaneously. Also, the proteopathic state $(u_4, \widetilde{u}_4, v_4, \widetilde{v}_4)$ exists if $b_0/b_1 > v_4$ holds. Since, $\widetilde{u}_4 = \widetilde{u}_3$, we can choose b_3 in such a way that $b_3\widetilde{u}_4 - e_2\widetilde{b}_1 + b_2 \geq 0$. Therefore, to produce tau proteopathy, the stationary state $(u_2, \widetilde{u}_2, v_2, \widetilde{v}_2)$ is not needed. So, we study only two types of patient proteopathies: (i) primary tauopathy and (ii) secondary tauopathy.

For the primary tauopathy, which is usually related to neurodegenerative diseases such as AD, all the four stationary states exist i.e., both the conditions $b_0/b_1 \geq \widetilde{b}_1/(b_2 - e_2\widetilde{b}_1)$ and $a_0/a_1 \geq \widetilde{a}_1/(a_2 - e_1\widetilde{a}_1)$ hold. In this case, we have plotted the dynamics of the system (3) in Fig. 2(a). Also, for the secondary tauopathy, only three stationary states exist. Here, the inequality $a_0/a_1 \geq \widetilde{a}_1/(a_2 - e_1\widetilde{a}_1)$ is true and the other inequality fails. An example of secondary tauopathy is shown in Fig. 2(b). Comparing the homogeneous systems corresponding to (1) and (2), the modified system requires less toxic load.
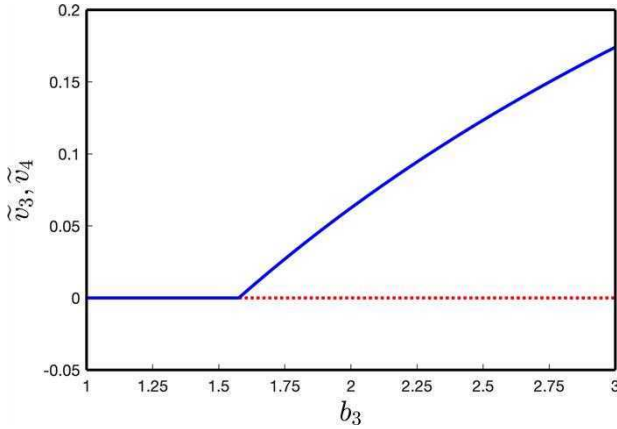
Fig. 1. Transcritical bifurcation diagram of the stationary points for the system (3). (Parameter values: $a_0 = a_1 = a_2 = b_0 = b_1 = b_2 = 1, \widetilde{a}_1 = 3/4, \widetilde{b}_1 = 4/3, e_1 = e_2 = 0.1$.)
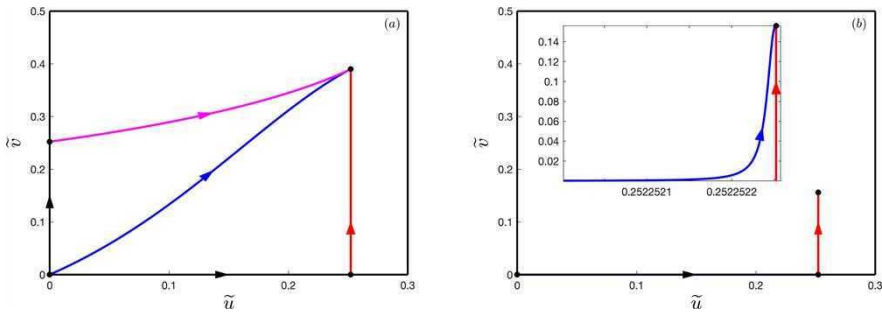
Fig. 2. Phase plane $(\widetilde{u}, \widetilde{v})$ with four and three stationary points for the system (3): (a) $\widetilde{b}_1 = 3/4, b_3 = 0.5$ and (b) $\widetilde{b}_1 = 4/3, b_3 = 3$. (Parameter values: $a_0 = a_1 = a_2 = b_0 = b_1 = b_2 = 1, \widetilde{a}_1 = 3/4, e_1 = e_2 = 0.1$.)

For the wave propagation, we consider the spatial domain in one dimension $[-100, 100]$ as an example. However, the results are robust for a wide range of intervals. We take the initial condition $(u(x,0), \widetilde{u}(x,0), v(x,0), \widetilde{v}(x,0))$ for the primary tauopathy as $(u_3, \widetilde{u}_3, v_3, \widetilde{v}_3)$ for $-100 \leq x \leq -95$, $(u_1, \widetilde{u}_1, v_1, \widetilde{v}_1)$ for $-95 < x < 95$ and $(u_2, \widetilde{u}_2, v_2, \widetilde{v}_2)$ for $95 \leq x \leq 100$. On the other hand, the initial condition $(u(x,0), \widetilde{u}(x,0), v(x,0), \widetilde{v}(x,0))$ for the secondary tauopathy has been taken as $(u_3, \widetilde{u}_3, v_3, \widetilde{v}_3)$ for $-100 \leq x \leq -95$, $(u_1, \widetilde{u}_1, v_1, \widetilde{v}_1)$ for $-95 < x < 95$ and $(u_2, \widetilde{u}_2, v_2, 10^{-6})$ for $95 \leq x \leq 100$.

We have shown the wave propagation for the primary tauopathy in Fig. 3 at different time steps $t = 50, 150, 180$ and 220. Motivated by Thompson et al., we have chosen the parameter values as $a_0 = a_1 = a_2 = b_0 = b_1 = b_2 = 1, \widetilde{a}_1 = \widetilde{b}_1 = 3/4, b_3 = 0.5, e_1 = e_2 = 0.1, d_1 = \widetilde{d}_1 = d_2 = \widetilde{d}_2 = 1$ and no-flux
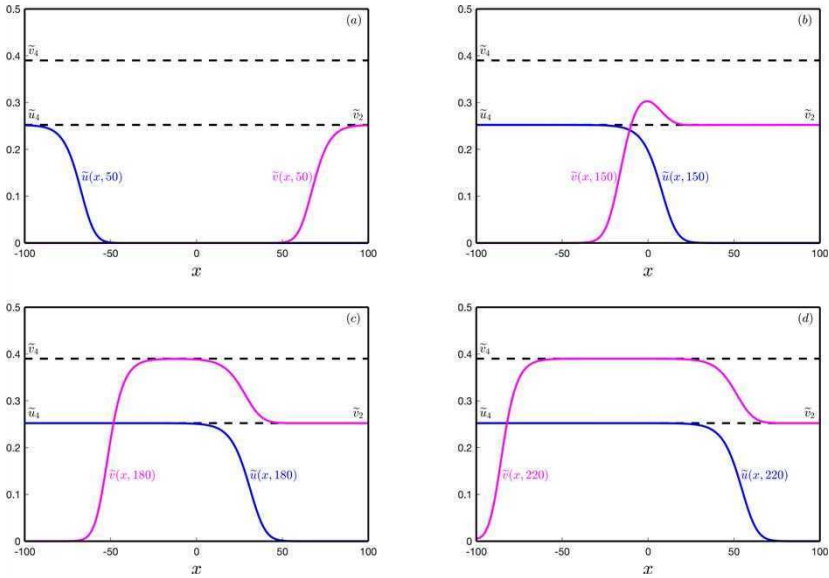
Fig. 3. Front propagations of $\widetilde{u}$ and $\widetilde{v}$ for the system (2) at different time steps: (a) $t = 50$, (b) $t = 150$, (c) $t = 180$ and (d) $t = 220$.

boundary conditions for all the variables. For these parametric values, we obtain $c_\beta^{(14)} = c_\tau^{(12)} = c_\tau^{(14)} = 0.798$ and $c_\tau^{(34)} = 1.068$. In the simulation, we have considered the toxic $A\beta$ front on the left side of the domain and toxic τP on the right. Initially, the toxic $A\beta$ front propagates to the right with speed $c_\beta^{(14)}$ and toxic τP propagates to the left with speed $c_\tau^{(12)}$. After overlapping both the fronts, τP increases its concentration and connects to $\widetilde{v}_4$. Then, the left front of the wave of τP boosts its speed to $c_\tau^{(34)}$ and moves to the left. On the other hand, the right front of the wave of τP moves with speed $c_\tau^{(14)}$, it eventually fills the domain and the entire system converges to the stable equilibrium solution $(u_4, \widetilde{u}_4, v_4, \widetilde{v}_4)$.

In Fig. 4, we plot wave propagation for the secondary tauopathy at different time steps $t = 60, 250, 400$ and 425. We have chosen the parameter values as $a_0 = a_1 = a_2 = b_0 = b_1 = b_2 = 1, \widetilde{a}_1 = 3/4, \widetilde{b}_1 = 4/3, b_3 = 3, e_1 = e_2 = 0.1, d_1 = \widetilde{d}_1 = d_2 = \widetilde{d}_2 = 1$ and no-flux boundary conditions for all the variables. For these parametric values, we obtain $c_\beta^{(14)} = 0.798$ and $c_\tau^{(34)} = 1.153$. Here, the toxic $A\beta$ front propagates to the right with speed $c_\beta^{(14)}$ and fills the domain $\widetilde{u}_4$ with negligible toxic τP (see Fig. 2(b)). However, we note that after filling toxic $A\beta$ in the entire domain, toxic τP starts to increase its concentration and connects to $\widetilde{v}_4$. It moves with the speed $c_\tau^{(34)}$ and fills the domain. Finally, the entire system converge to the stable equilibrium solution $(u_4, \widetilde{u}_4, v_4, \widetilde{v}_4)$.
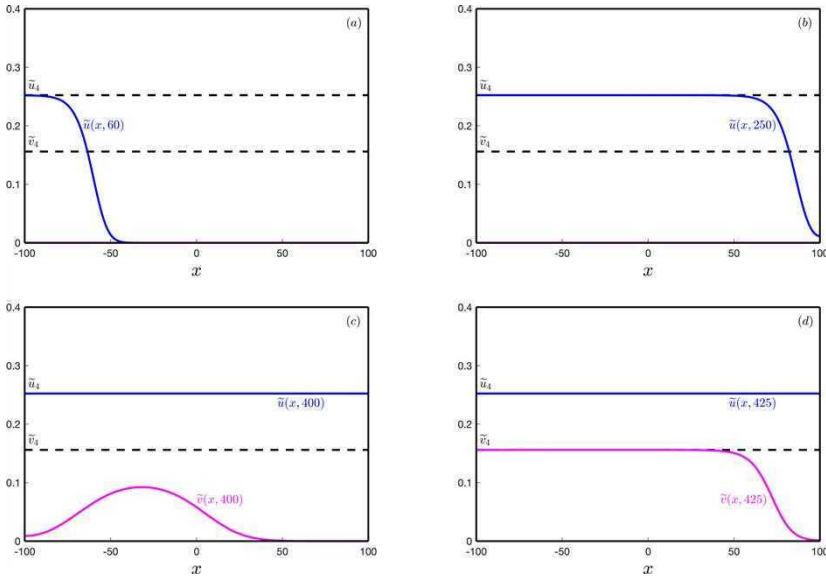
Fig. 4. Front propagations of $\widetilde{u}$ and $\widetilde{v}$ for the system (2) at different time steps: (a) $t = 60$, (b) $t = 250$, (c) $t = 400$ and (d) $t = 425$.

For the network model, brain connectome data is available with different resolutions in, e.g., [14]: the lowest resolution consists of 83 nodes, and the highest resolution consists of 1015 nodes. However, there is some difference in the staging area of $A\beta$ and τP in the brain connectome. A more general approach to the analysis of brain hubs in human connectomes has recently been proposed in [27]. In the context of our research on the pathology dynamics, the network model (14) can be solved numerically for the given number of nodes with non-negative initial conditions. Furthermore, we can extend our analysis on primary and secondary tauopathies for the network model as well. Finally, we note that in the analysis currently being undertaken, not only we can choose uniform parameter values for all the nodes but also different parameter values in different regions in the brain connectome, as required by a more detailed study.

7   Conclusion

We have studied a modification of the heterodimer model, which captures the conversion time from healthy to toxic proteins. For the temporal dynamics, we have carried out the linear stability analysis of all the stationary points. We have also investigated the wave speeds of the travelling wavefronts for the spatio-temporal model. Further, a computationally challenging network mathematical model has been described based on a coarse-graining procedure of the continuous model and taking advantage of the brain data connectome. In this latter model the edges of the network are the axonal bundles in white-matter tracts.

We have highlighted an efficient way to analyze such models in the context of neurodegenerative diseases such as AD.

We have obtained two clinically interesting patient proteopathies for further detailed analysis: primary and secondary tauopathies. For the case of primary tauopathy, a possible invasion of τP exists independent of the invasion of $A\beta$. On the other hand, for the secondary tauopathy, the sustained presence of toxic τP requires the company of toxic $A\beta$. These conclusions are similar for both the models (heterodimer and the modified version). However, for the same parametric values, the introduction of Holling type-II functional response decreases the concentrations of toxic τP and toxic $A\beta$ compared to the original model. Finally, a detailed analysis of different tauopathies with non-uniform parameters has been recently carried out in [28] with further developments of the network model reported here.

References

1. Alzheimer, A.: Uber eine eigenartige Erkrankung der Hirnrinde. Zentralbl Nervenh Psych. **18**, 177–179 (1907)
2. Hardy, J.A., Higgins, G.A.: Alzheimer's disease: the amyloid cascade hypothesis. Science **256**, 184–186 (1992)
3. Hardy, J., Allsop, D.: Amyloid deposition as the central event in the aetiology of Alzheimer's disease. Trends Pharmacol. Sci. **12**, 383–388 (1991)
4. Gotz, J., Halliday, G., Nisbet, R.M.: Molecular pathogenesis of the tauopathies. Annu. Rev. Pathol. **14**, 239–261 (2019)
5. Cho, H., et al.: In vivo cortical spreading pattern of tau and amyloid in the Alzheimer disease spectrum. Ann. Neurol. **80**, 247–258 (2016)
6. Jack, C.R., et al.: NIA-AA research framework: toward a biological definition of Alzheimer's disease. Alzheimer's Dementia **14**, 535–562 (2018)
7. DeVos, S.L., et al.: Tau reduction in the presence of amyloid $-\beta$ prevents tau pathology and neuronal death in vivo. Brain **141**, 2194–2212 (2018)
8. Busche, M.A., et al.: Tau impairs neural circuits, dominating amyloid $-\beta$ effects, in Alzheimer models in vivo. Threshold **30**, 50 (2019)
9. Walker, L.C., Lynn, D.G., Chernoff, Y.O.: A standard model of Alzheimer's disease? Prion **12**, 261–265 (2018)
10. Ittner, L.M., Gotz, J.: Amyloid-β and tau-a toxic pas de deux in Alzheimer's disease. Nature Rev. Neurosci. **12**, 67 (2011)
11. Jack, Jr. C.R., et al.: Tracking pathophysiological processes in Alzheimer's disease: an updated hypothetical model of dynamic biomarkers. Lancet Neurol. **12**, 207–216 (2013)
12. Kara, E., Marks, J.D., Aguzzi, A.: Toxic protein spread in neurodegeneration: reality versus fantasy. Trends in Molecular Medicine (2018)
13. Vosoughi, A., et al.: Mathematical models to shed light on amyloid-beta and tau protein dependent pathologies in Alzheimer's disease. Neuroscience **424**, 45–57 (2020)
14. Thompson, T.B., Chaggar, P., Kuhl, E., Goriely, A.: Protein-protein interactions in neurodegenerative diseases: a conspiracy theory. PLoS Comput. Biol. **16**, e1008267 (2020)

15. Fornari, S., Schäfer, A., Goriely, A., Kuhl, E.: Prion-like spreading of Alzheimer's disease within the brain's connectome. Interface R Society **16**, 20190356 (2019)

16. Fornari, S., Schäfer, A., Kuhl, E., Goriely, A.: Spatially-extended nucleation-aggregation-fragmentation models for the dynamics of prion-like neurodegenerative protein-spreading in the brain and its connectome. J. Theor. Biol. **486**, 110102 (2020)

17. Jucker, M., Walker, L.C.: Pathogenic protein seeding in Alzheimer disease and other neurodegenerative disorders. Ann. Neurol. **70**, 532–540 (2011)

18. Zheng, Y.Q., et al.: Local vulnerability and global connectivity jointly shape neurodegenerative disease propagation. PLoS Biol. **17**(11), e3000495 (2019)

19. Insel, P., Mormino, E., Aisen, P., Thompson, W., Donahue, M.: Neuroanatomical spread of amyloid β and tau in Alzheimer's disease: implications for primary prevention. Brain Commun. **2**, 1–11 (2020)

20. Moreno-Jimenez, E., Flor-Garcia, M.: Adult hippocampal neurogenesis is abundant in neurologically healthy subjects and drops sharply in patients with Alzheimer's disease. Nat. Med. **25**, 554–560 (2019)

21. Bressloff, P.C.: Waves in Neural Media. Lecture Notes on Mathematical Modelling in the Life Sciences. Springer, New York (2014). https://doi.org/10.1007/978-1-4614-8866-8

22. Matthäus, F.: Comparison of modeling approaches for the spread of prion diseases in the brain. In: Mitkowski, W., Kacprzyk, J. (eds.) Modelling Dynamics in Processes and Systems, vol. 180, pp. 109–117. Springer, Heidelberg (2009). https://doi.org/10.1007/978-3-540-92203-2_8

23. Bertsch, M., Franchi, B., Marcello, N., Tesi, M.C., Tosin, A.: Alzheimer's disease: a mathematical model for onset and progression. Math. Med. Biol. **34**, 193–214 (2016)

24. Weickenmeier, J., Kuhl, E., Goriely, A.: The multiphysics of prion-like diseases: progression and atrophy. Phys. Rev. Lett. **121**, 264–281 (2018)

25. Weickenmeier, J., Jucker, M., Goriely, A., Kuhl, E.: A physics-based model explains the prion-like features of neurodegeneration in Alzheimer's disease, Parkinson's disease, and amyotrophic lateral sclerosis. J. Mech. Phys. Solids **124**, 264–281 (2019)

26. Dawes, J.H.P., Souza, M.O.: A derivation of Holling's type I, II and III functional responses in predator-prey systems. J. Theo. Bio. **327**, 11–22 (2013)

27. Tadic, B., Melnik, R., Andjelkovic, M.: The topology of higher-order complexes associated with brain hubs in human connectomes. Scientifc Rep. **10**, 17320 (2020)

28. Pal, S., Melnik, R.: Nonlocal multiscale interactions in brain neurodegenerative protein dynamics and coupled proteopathic processes. In: Onate, E., Papadrakakis, M., Schreflfler, B. (eds.) Proceedings of the IX International Conference on Computational Methods for Coupled Problems in Science and Engineering, CIMNE, Barcelona, Coupled problems 2021 (2021). 12 p.